

The role of the N-terminal domain in dimerization and nucleocytoplasmic shuttling of latent STAT3

Michael Vogt¹, Tamas Domszalai¹, Dzina Kleshchanok², Swen Lehmann², Anne Schmitt¹, Valeria Poli³, Walter Richtering² and Gerhard Müller-Newen^{1,*}

¹Institute of Biochemistry and Molecular Biology, Medical School, RWTH Aachen University, Pauwelsstrasse 30, Aachen 52074, Germany

²Institute of Physical Chemistry, RWTH Aachen University, Aachen 52056, Germany

³Department of Genetics, Biology and Biochemistry, Molecular Biotechnology Center, University of Turin, Torino 10126, Italy

*Author for correspondence (mueller-newen@rwth-aachen.de)

Accepted 15 October 2010

Journal of Cell Science 124, 900–909

© 2011. Published by The Company of Biologists Ltd

doi:10.1242/jcs.072520

Summary

STAT3 is an important transcription factor involved in immunity and cancer. In response to cytokine stimulation, STAT3 becomes phosphorylated on a single tyrosine residue. Tyrosine-phosphorylated STAT3 accumulates in the nucleus, binds to specific DNA response elements and induces gene expression. Unphosphorylated, latent STAT3 shuttles constitutively between cytoplasm and nucleus. We analysed the importance of previously identified putative nuclear localization sequences (NLS) and nuclear export sequences (NES) for nucleocytoplasmic shuttling of latent STAT3 using STAT3-deficient cells reconstituted with fluorescently labelled STAT3 mutants. Mutation of a putative NLS or NES sequence did not impair nucleocytoplasmic shuttling of latent STAT3. We were also interested in the structural requirements for dimerization of unphosphorylated STAT3 and its relevance for nucleocytoplasmic shuttling. By native gel electrophoresis and dual-focus fluorescence correlation spectroscopy (2f-FCS) we identified the N-terminal domain (amino acids 1–125) to be essential for formation of unphosphorylated STAT3 dimers but not for assembly of tyrosine-phosphorylated STAT3 dimers. In resting cells, the monomeric N-terminal deletion mutant (STAT3-ΔNT) shuttles faster between the cytoplasm and nucleus than the wild-type STAT3, indicating that dimer formation is not required for nucleocytoplasmic shuttling of latent STAT3. STAT3-ΔNT becomes phosphorylated and dimerizes in response to interleukin-6 stimulation but, surprisingly, does not accumulate in the nucleus. These results highlight the importance of the N-terminal domain in the formation of unphosphorylated STAT3 dimers and nuclear accumulation of STAT3 upon phosphorylation.

Key words: STAT3, Dimerization, Nucleocytoplasmic shuttling, Confocal microscopy, Dual-focus FCS

Introduction

The JAK/STAT (Janus tyrosine kinase/signal transducer and activator of transcription) signalling pathway is utilized by many cytokines and growth factors to rapidly transmit the signal from membrane-bound receptors to the nucleus. The membrane-proximal cytoplasmic part of cytokine receptors is associated with JAKs. Upon activation by the ligand, the JAKs phosphorylate cytoplasmic tyrosine residues of the cytokine receptors. These phosphotyrosine residues serve as docking sites for signalling molecules with an SH2 domain, such as STAT transcription factors. STATs are recruited to the receptor and become phosphorylated on a single tyrosine residue by the JAKs. Phosphorylated STATs dimerize by reciprocal phosphotyrosine–SH2 domain interactions and translocate into the nucleus where they induce target genes (Levy and Darnell, 2002).

This canonical view of JAK/STAT signalling has been refined with regard to dimerization and nuclear translocation of STAT transcription factors. It has been firmly established that many if not all STAT proteins exist as preformed dimers in the absence of the activating tyrosine phosphorylation (Braunstein et al., 2003). However, the molecular interfaces that drive dimerization differ between individual STATs. In this respect, STAT1 has been most thoroughly investigated (Mao et al., 2005). All STAT proteins are built up similarly. They consist of an N-terminal domain, a coiled-coil domain, the DNA-binding domain, a linker domain, a SH2 domain and, finally, the transactivation domain. A STAT protein lacking the N-terminal domain and the C-terminal transactivation

domain is often referred to as ‘core fragment’. Dimerization of unphosphorylated STAT1 is mediated by homotypic interactions of the N-terminal domains and reciprocal interactions of the core fragment, resulting in an anti-parallel orientation (Mao et al., 2005). Also, STAT3 is a dimeric protein in the absence of phosphorylation (Haan et al., 2000). Although the core fragment of STAT1 contributes to dimerization, the core fragment of STAT3 is a monomeric protein (Ren et al., 2008). Thus, the N-terminal domain or the transactivation domain must be involved in the formation of unphosphorylated STAT3 dimers.

STATs are often described as latent cytoplasmic transcription factors that enter the nucleus in response to tyrosine phosphorylation. It is true that tyrosine phosphorylation of STATs leads to their nuclear accumulation. However, non-phosphorylated STATs are also able to enter the nucleus. They shuttle permanently between the cytoplasm and the nucleus, resulting in a steady-state of high cytoplasmic and low nuclear STAT concentrations (Meyer and Vinkemeier, 2004). This nucleocytoplasmic shuttling of latent STATs is amazingly fast for, e.g. STAT2 (Frahm et al., 2006) but quite slow for STAT3 (Pranada et al., 2004).

Among the seven mammalian STAT proteins (STAT1, STAT2, STAT3, STAT4, STAT5A, STAT5B, STAT6), STAT3 has the most pleiotropic functions (Levy and Lee, 2002). Its knockout leads to early embryonic lethality, which points to a role of STAT3 in embryonic development. In the adult, STAT3 is an important transcription factor in immunity and inflammation. Dysregulated STAT3 activation is implicated in chronic inflammation and cancer

(Yu and Jove, 2004). In this study, we have investigate the structural requirements for dimerization and nucleocytoplasmic shuttling of latent STAT3.

Results

Analysis of nucleocytoplasmic shuttling of STAT3 using the STAT3–CY construct

For the analysis of nucleocytoplasmic shuttling we generated a STAT3 construct termed STAT3–CY that is C-terminally tagged

with the cyan (CFP) and yellow (YFP) fluorescent proteins. Using the 514 nm laser of a confocal microscope, YFP can be selectively bleached without damaging CFP (Fig. 1A). A shuttling assay in living cells has been developed that is based on the cytoplasmic bleaching of YFP and detection of YFP and CFP fluorescence in cytoplasmic and nuclear regions of interests (ROIs). A decrease of nuclear YFP fluorescence is indicative of shuttling, with the CFP fluorescence serving as an internal standard (Fig. 1B). Using this assay, nucleocytoplasmic shuttling of latent STAT3 (Pranada et al.,

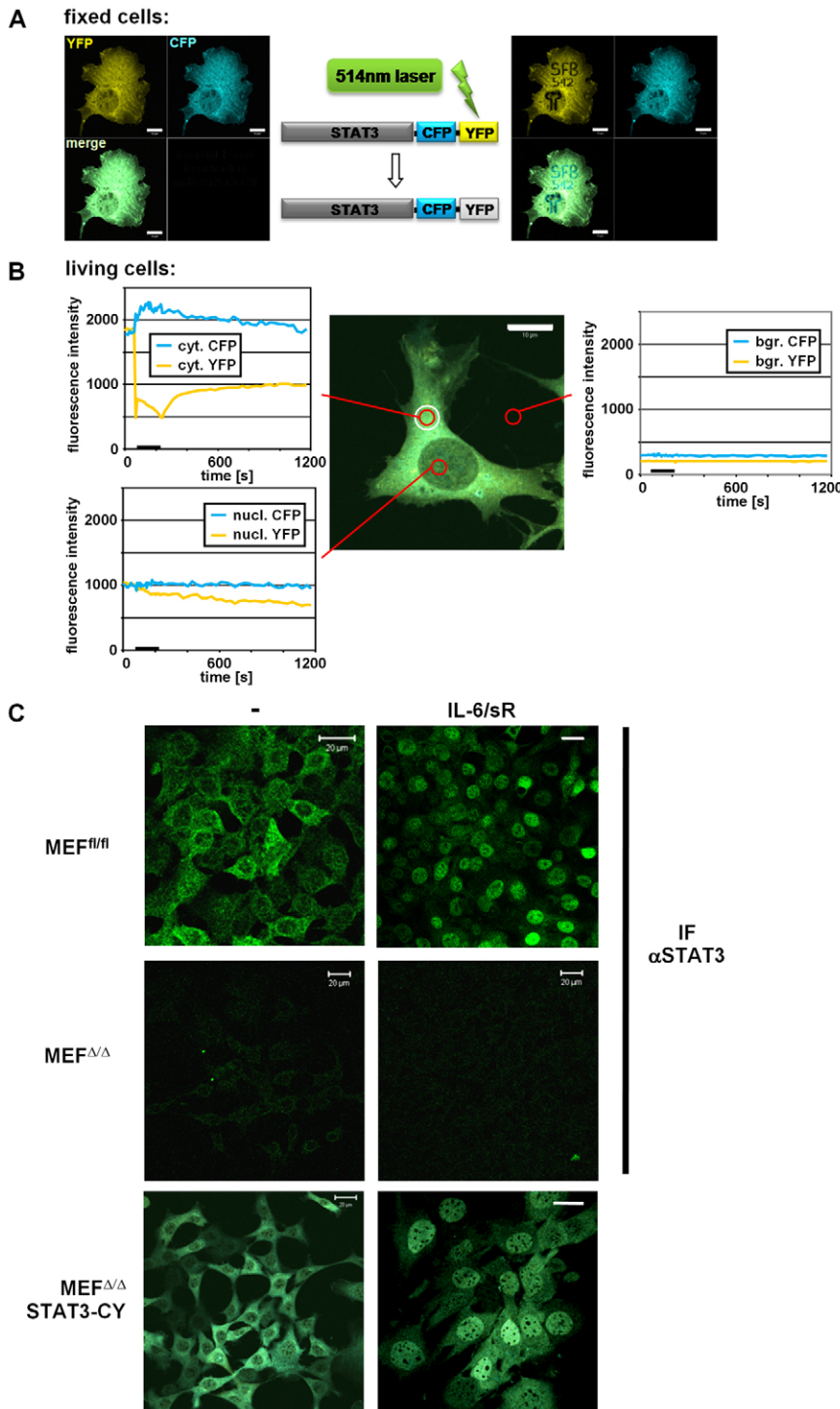


Fig. 1. Analysis of nucleocytoplasmic shuttling using STAT3–CY. (A) Selective bleaching of YFP in STAT3–CY. MEF ^{$\Delta\Delta$} stably transfected with STAT3–CY were fixed and images of a single cell were taken using the YFP and the CFP channels of a confocal microscope. A pattern was bleached representing the lettering and icon of the Collaborative Research Center SFB 542 using the 514 nm laser of the confocal microscope. Subsequently, images were taken under the same conditions as before bleaching. The bleached pattern is only visible in the YFP channel. The CFP fluorescence is unaffected by the bleaching procedure. Scale bars: 10 μ m. (B) Setup of the shuttling assay. Nucleocytoplasmic shuttling was analysed in single living MEF ^{$\Delta\Delta$} cells stably transfected with STAT3–CY constructs. For this purpose, the YFP moiety of STAT3–CY was irreversibly bleached in a cytoplasmic ROI (white circle). CFP and YFP fluorescence was monitored in a cytoplasmic ROI, a nuclear ROI and an extracellular ROI for the detection of background fluorescence (red circles). The CFP and YFP fluorescence measured are depicted in the diagrams. The transient increase of CFP fluorescence in the cytoplasmic ROI is a result of the loss of FRET between CFP and YFP upon bleaching of YFP. The CFP signal decreases over time because of redistribution of the bleached molecules within the cytoplasm. Decay of nuclear YFP fluorescence in the presence of a constant CFP signal is indicative of nucleocytoplasmic shuttling of STAT3–CY. Scale bar: 10 μ m. (C) Subcellular localization of endogenous STAT3 and fluorescently labelled STAT3–CY. MEF^{fl/fl}, MEF ^{$\Delta\Delta$} and MEF ^{$\Delta\Delta$} stably transfected with STAT3–CY (MEF ^{$\Delta\Delta$} STAT3–CY) were stimulated with 20 ng/ml IL-6 and 0.5 μ g/ml soluble IL-6R (sR) for 30 minutes or left untreated. All cells were fixed. MEF^{fl/fl} and MEF ^{$\Delta\Delta$} were permeabilized and prepared for immunofluorescence (IF) using a STAT3 antibody, followed by incubation with a Cy2-labelled secondary antibody. Cells were analysed by confocal microscopy. Scale bars: 20 μ m.

2004) as well as of persistently activated STAT3 (Herrmann et al., 2007) has been established.

The subcellular distribution of endogenous STAT3 and ectopically expressed STAT3–CY in murine embryonic fibroblasts (MEF) was compared (Fig. 1C). MEF with floxed STAT3 alleles (MEF^{fl/fl}) and MEF lacking STAT3 (MEF^{Δ/Δ}) were analysed by immunofluorescence using a STAT3 antibody. In non-stimulated cells, endogenous STAT3 was preferentially located in the cytoplasm but nuclear STAT3 was also detectable. Upon interleukin-6 (IL-6) stimulation, the distribution was inverted with most of the STAT3 appearing in the nucleus and low amounts remaining in the cytoplasm (Fig. 1C, upper panel). MEF^{Δ/Δ} were analysed under identical settings to control specificity of the staining. Only a weak background signal was detectable (Fig. 1C, middle panel). The subcellular distributions of STAT3–CY in stably transfected MEF^{Δ/Δ} and endogenous STAT3 in MEF^{fl/fl} were comparable before as well as after stimulation (Fig. 1C, compare upper and lower panels). Thus, the CY-tag has no major influence on the subcellular distribution of STAT3.

Nucleocytoplasmic shuttling of putative NLS and NES mutants of STAT3

MEF^{Δ/Δ} were stably transfected with STAT3–CY mutants (Fig. 2A) to analyse the importance of putative nuclear localization sequences (NLS) and nuclear export sequences (NES) for nucleocytoplasmic shuttling. Lysates of these cells were prepared before and after IL-6 stimulation and analysed for STAT3 expression and phosphorylation by immunoblotting (Fig. 2B). STAT3-ΔNLS–CY (with point mutations of arginines 214 and 215 to alanine) and STAT3-ΔNES–CY (with leucines 525 and 528 exchanged for alanine) were phosphorylated on tyrosine 705 in response to IL-6 stimulation, as were STAT3–CY in MEF^{Δ/Δ} and endogenous STAT3 in MEF^{fl/fl}. STAT3–CY and the mutants showed the expected apparent molecular mass of 145 kDa.

The subcellular distribution of the mutants was analysed by confocal microscopy. In non-stimulated cells, the distribution of STAT3-ΔNLS–CY was indistinguishable from STAT3–CY (Fig. 2C, upper and middle panels). However, upon phosphorylation STAT3-ΔNLS–CY does not accumulate in the nucleus. Compared to the wild-type, the distribution of STAT3-ΔNES–CY in non-stimulated cells was shifted to the nucleus. STAT3-ΔNES–CY responded to IL-6 stimulation with nuclear accumulation (Fig. 2C, lower panel). Thus, the STAT3 mutants that were double-labelled with CFP and YFP behaved as previously reported for the single-tagged proteins (Bhattacharya and Schindler, 2003; Ma et al., 2003).

The dynamic behaviour of the NLS and NES mutants was analysed in the shuttling assay described above. For clarity, in the diagrams in Fig. 3, the YFP fluorescence in the cytoplasmic and nuclear ROIs is depicted but not the CFP fluorescence. Only those experiments were evaluated in which the CFP fluorescence in the nuclear ROI did not change during the measurement. Comparison of STAT3–CY (Fig. 3A) and STAT3-ΔNLS–CY (Fig. 3B) revealed that mutation of the putative NLS sequence of STAT3 does not have any impact on nucleocytoplasmic shuttling. STAT3-ΔNES–CY also shuttles between the cytoplasm and the nucleus. Unexpectedly, the rate of nucleocytoplasmic shuttling was even increased, as indicated by the more rapid decrease of nuclear YFP fluorescence in response to cytoplasmic bleaching. Fig. 3D shows an important control experiment proving that data recording alone does not contribute to any significant bleaching of the fluorophores. Thus, previously identified putative NLS and NES sequences of

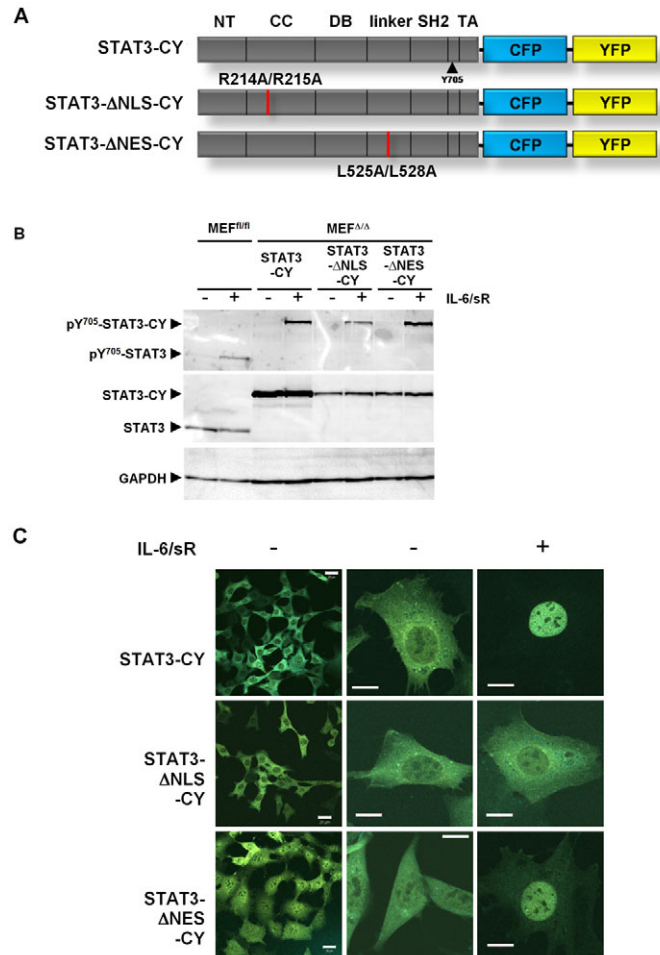


Fig. 2. Characterization of STAT3–CY and putative NLS and NES mutants. (A) Representation of the domain structure of STAT3–CY and mutants used for the generation of stable cell lines. Red bars show the positions of the indicated point mutations. NT, N-terminal domain; CC, coiled-coil domain; DB, DNA-binding domain; SH2, src-homology 2 domain; TA, transactivation domain. (B) MEF^{Δ/Δ} stably transfected with STAT3–CY, STAT3-ΔNLS–CY or STAT3-ΔNES–CY, or MEF^{fl/fl}, were stimulated with 20 ng/ml IL-6 and 0.5 μg/ml soluble IL-6R (sR) for 30 minutes or left untreated. Cellular lysates were analysed by immunoblotting using antibodies against phosphotyrosine 705 of STAT3, STAT3 and GAPDH as a loading control. (C) MEF^{Δ/Δ} stably transfected with STAT3–CY, STAT3-ΔNLS–CY or STAT3-ΔNES–CY were stimulated with 20 ng/ml IL-6 and 0.5 μg/ml soluble IL-6R (sR) for 30 minutes or left untreated. Cells were fixed and analysed by confocal microscopy. Scale bars: 20 μm.

STAT3 are not required for nucleocytoplasmic shuttling of latent STAT3.

Dimerization of latent STAT3–CY analysed by native gel electrophoresis

It has been firmly established that STAT3 and other STAT proteins form dimers in the absence of tyrosine phosphorylation (Braunstein et al., 2003; Haan et al., 2000). To assess the importance of dimerization for the nucleocytoplasmic shuttling of latent STAT3 we wanted to compare the shuttling of wild-type and monomeric mutants of STAT3. As outlined in the Introduction, structural investigations of STAT1 (Mao et al., 2005) and STAT3 (Ren et al.,

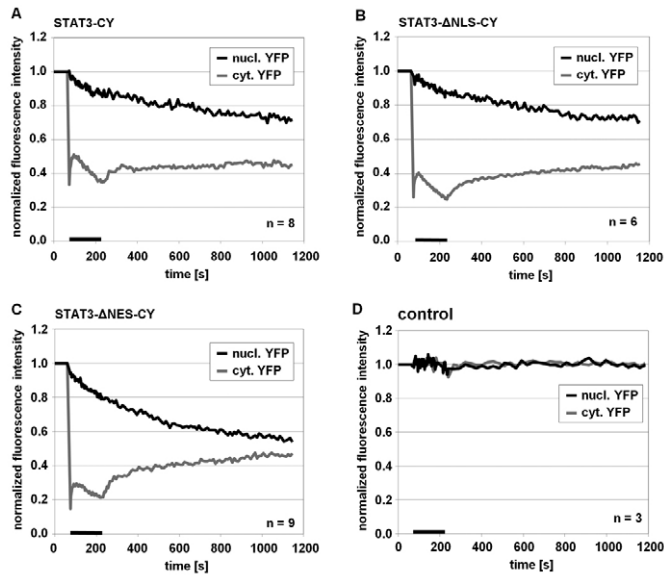


Fig. 3. Nucleocytoplasmic shuttling of wild-type and mutant STAT3 in stably transfected MEF $\Delta\Delta$. (A–C) The shuttling assay was performed in single living MEF $\Delta\Delta$ cells stably transfected with STAT3–CY (A), STAT3– Δ NLS–CY (B) and STAT3– Δ NES–CY (C) at a confocal microscope, as described for Fig. 1B. Living cells were analysed in an incubation chamber at 37°C. The diagrams show the normalized and then averaged cytoplasmic and nuclear YFP fluorescence over time from n experiments as indicated. The bars at the x -axis represent the duration of the cytoplasmic bleach pulses. Only experiments with constant nuclear CFP fluorescence (not shown) were evaluated. (D) In this control experiment, the same cells as in A were used but the bleach-ROI was located outside of the cell. The constant YFP fluorescence in the cytoplasmic and nuclear ROIs indicate that data recording does not contribute to bleaching of the fluorophore.

2008) indicate that the N-terminal domain of STAT3 might be essential for dimerization.

To test the above hypothesis, a deletion mutant of STAT3–CY lacking the N-terminal domain of STAT3 (STAT3– Δ NT–CY) was generated. Another mutant (STAT3–VL–CY) with two amino acids exchanged (valine 77 and leucine 78 both exchanged for alanine) in the N-terminal domain was designed in analogy to a dimerization-deficient STAT1 mutant (Fig. 4A). Lysates of stably transfected MEF $\Delta\Delta$ were analysed by immunoblotting (Fig. 4B). Both mutants were tyrosine-phosphorylated in response to stimulation with IL-6. The counterstaining of STAT3 revealed the expected increased electrophoretic mobility of the deletion mutant STAT3– Δ NT–CY compared to STAT3–VL–CY.

In a first approach, the native molecular masses of the different STAT3–CY constructs were compared by blue-native PAGE (bnPAGE) of cellular lysates prepared under mild detergent conditions. After electrophoresis, the gel was analysed with a fluorescence scanner visualizing only the fluorescently labelled proteins (Fig. 4C). Therefore, lysates of non-transfected MEF $\Delta\Delta$ displayed no signals. Lysates of non-stimulated MEF $\Delta\Delta$ expressing STAT3–CY showed two bands, one representing the STAT3–CY monomer, the other representing the dimer. Interestingly the dimer:monomer ratio did not change much upon stimulation. By contrast, non-phosphorylated STAT3– Δ NT–CY was a strictly monomeric protein. However, upon stimulation a fraction of dimers was generated. Dimerization of STAT3–VL–CY seemed to be

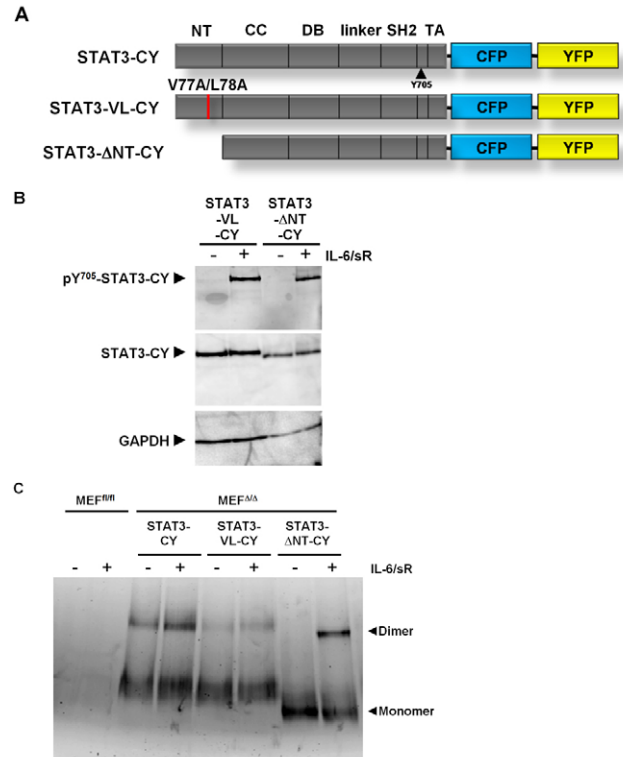


Fig. 4. Role of the N-terminal domain in dimerization of STAT3.

(A) Representation of the domain structure of STAT3–CY and mutants used for the generation of stable cell lines. The red bar shows the position of the indicated point mutations. NT, N-terminal domain; CC, coiled-coil domain; DB, DNA-binding domain; SH2, src-homology 2 domain; TA, transactivation domain. (B) MEF $\Delta\Delta$ stably transfected with STAT3–VL–CY or STAT3– Δ NT–CY were stimulated with 20 ng/ml IL-6 and 0.5 μ g/ml soluble IL-6R (sR) for 30 minutes or left untreated. Cellular lysates were analysed by immunoblotting using antibodies against phosphotyrosine 705 of STAT3, STAT3 and GAPDH as a loading control. (C) MEF $\Delta\Delta$ stably transfected with STAT3–CY, STAT3–VL–CY or STAT3– Δ NT–CY, or MEF $\Delta\Delta$, were stimulated with 25 ng/ml IL-6 and 0.5 μ g/ml soluble IL-6R (sR) for 30 minutes or left untreated. After mild lysis (0.5% Brij-96V) of the cells, 30 μ g of protein were incubated with Coomassie Brilliant blue G-250 and separated on a native gradient gel (4–20% PAA). The wet gel was analysed on a fluorescence scanner.

affected to some extent by the point mutations but was not abolished.

Dimerization of latent STAT3–eGFP analysed by fluorescence correlation spectroscopy

Dimerization of STAT3 and STAT3– Δ NT was further analysed by the recently established technique of dual-focus fluorescence correlations spectroscopy (2f-FCS). The basic concept of 2f-FCS is to use two laterally shifted and overlapping foci with a fixed and well-known distance serving as an external ruler during the experiment. By measuring the autocorrelation function (ACF) from each foci and the dual-focus cross-correlation function (CCF) between both foci, and analysing these functions, one can calculate the absolute values of the diffusion coefficient without further referencing or calibration (Dertinger et al., 2007; Müller et al., 2008).

For this purpose, eGFP-labelled constructs were generated. COS-7 cells were transiently transfected with STAT3–eGFP,

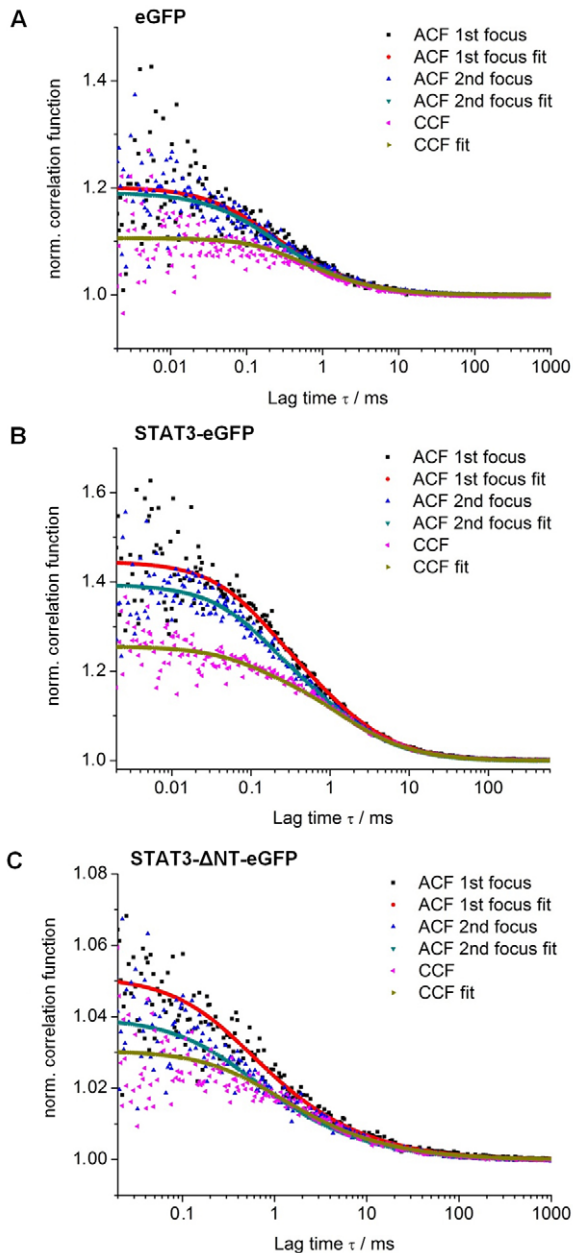


Fig. 5. Analysis of eGFP, STAT3-eGFP and STAT3- Δ NT-eGFP by 2f-FCS. (A–C) Auto- and cross-correlation functions (ACF and CCF, respectively) from 2f-FCS experiments on eGFP (A), STAT3-eGFP (B) and STAT3- Δ NT-eGFP (C). Experimental data points were fitted (lines) using a single particle diffusion model including triplet state correction.

STAT3- Δ NT-eGFP and eGFP as a control. Lysates of these cells were prepared and analysed by 2f-FCS. A representative autocorrelation function of each construct is shown in Fig. 5. Evaluation of the autocorrelation function of eGFP (Fig. 5A) by a one-component fitting model resulted in a diffusion coefficient of $1.03 \pm 0.04 \times 10^{-6} \text{ cm}^2/\text{s}$, which is in good agreement with published data (Kim and Schwille, 2003). An equivalent evaluation of the autocorrelation functions of STAT3-eGFP (Fig. 5B) and STAT3- Δ NT-eGFP (Fig. 5C) resulted in diffusion coefficients of 0.54 ± 0.08 and $0.7 \pm 0.03 \times 10^{-6} \text{ cm}^2/\text{s}$, respectively. From the diffusion coefficients, the hydrodynamic radii according to the Stokes-Einstein relation can be obtained. In addition, the molecular masses of the STAT3 proteins were calculated based on the diffusion coefficient and the known molecular mass of eGFP (Table 1). The resulting molecular mass of STAT3- Δ NT-eGFP ($88 \pm 11 \text{ kDa}$) is in good agreement with the predicted molecular mass of the STAT3- Δ NT-eGFP monomer (99 kDa). The apparent molecular mass of STAT3-eGFP ($216 \pm 99 \text{ kDa}$) fits with the predicted molecular mass of a STAT3-eGFP dimer (236 kDa). It was not possible to discriminate between a monomeric and a dimeric fraction of STAT3-eGFP due to limitations of the method. However, the high standard deviations in the measurements of STAT3-eGFP might be a consequence of a mixed population of monomers and dimers. Taken together, the results show that STAT3-eGFP forms dimers and the deletion of the N-terminal domain results in a purely monomeric population in resting cells.

Nucleocytoplasmic shuttling of monomeric STAT3

The subcellular distribution of STAT3-CY, STAT3- Δ NT-CY and STAT3-VL-CY in MEF $\Delta\Delta$ was analysed by confocal microscopy (Fig. 6A). Compared to wild-type, the deletion mutant STAT3- Δ NT-CY exhibited a more uniform distribution in non-stimulated cells. Most interestingly, STAT3- Δ NT-CY did not accumulate in the nucleus upon IL-6 stimulation, although this mutant became tyrosine phosphorylated (Fig. 4B), formed dimers upon phosphorylation (Fig. 4C), and bound to DNA (Fig. 6B). Lack of nuclear accumulation of STAT3- Δ NT-CY in response to stimulation has also been observed in transiently transfected MEF $\Delta\Delta$ and HEK293 cells as well as for non-tagged STAT3- Δ NT in transiently transfected MEF $\Delta\Delta$ (data not shown). STAT3-VL-CY resembles STAT3-CY with respect to the subcellular distribution in unstimulated cells and nuclear accumulation upon stimulation.

Nucleocytoplasmic shuttling of STAT3-CY, STAT3- Δ NT-CY, STAT3-VL-CY and CFP-YFP as a control in MEF $\Delta\Delta$ was analysed by iFLAP imaging as previously described (Herrmann et al., 2007). In this assay, the equal signals of CFP and YFP in the double-labelled constructs are transformed to zero by a simple algorithm, as exemplified for STAT3-CY (Fig. 6C, upper panels). As a

Table 1. Diffusion coefficients and average molecular masses derived from 2f-FCS experiments

Protein	Number of measurements	Diffusion coefficient ($\times 10^{-6}$) ($\text{cm}^2/\text{second}$)	Hydrodynamic radius (nm)	Average molecular mass (kDa)	Predicted molecular mass (kDa)
eGFP	3	1.03 ± 0.04	2.4 ± 0.1	–	27
STAT3-eGFP	12	0.54 ± 0.08	4.6 ± 0.8	216 ± 99	236 (dimer)
STAT3- Δ NT-eGFP	10	0.70 ± 0.03	3.5 ± 0.2	88 ± 11	99 (monomer)

The total number of measurements from three independent samples per construct are given. The predicted molecular masses were calculated from the known amino acid sequences of the proteins.

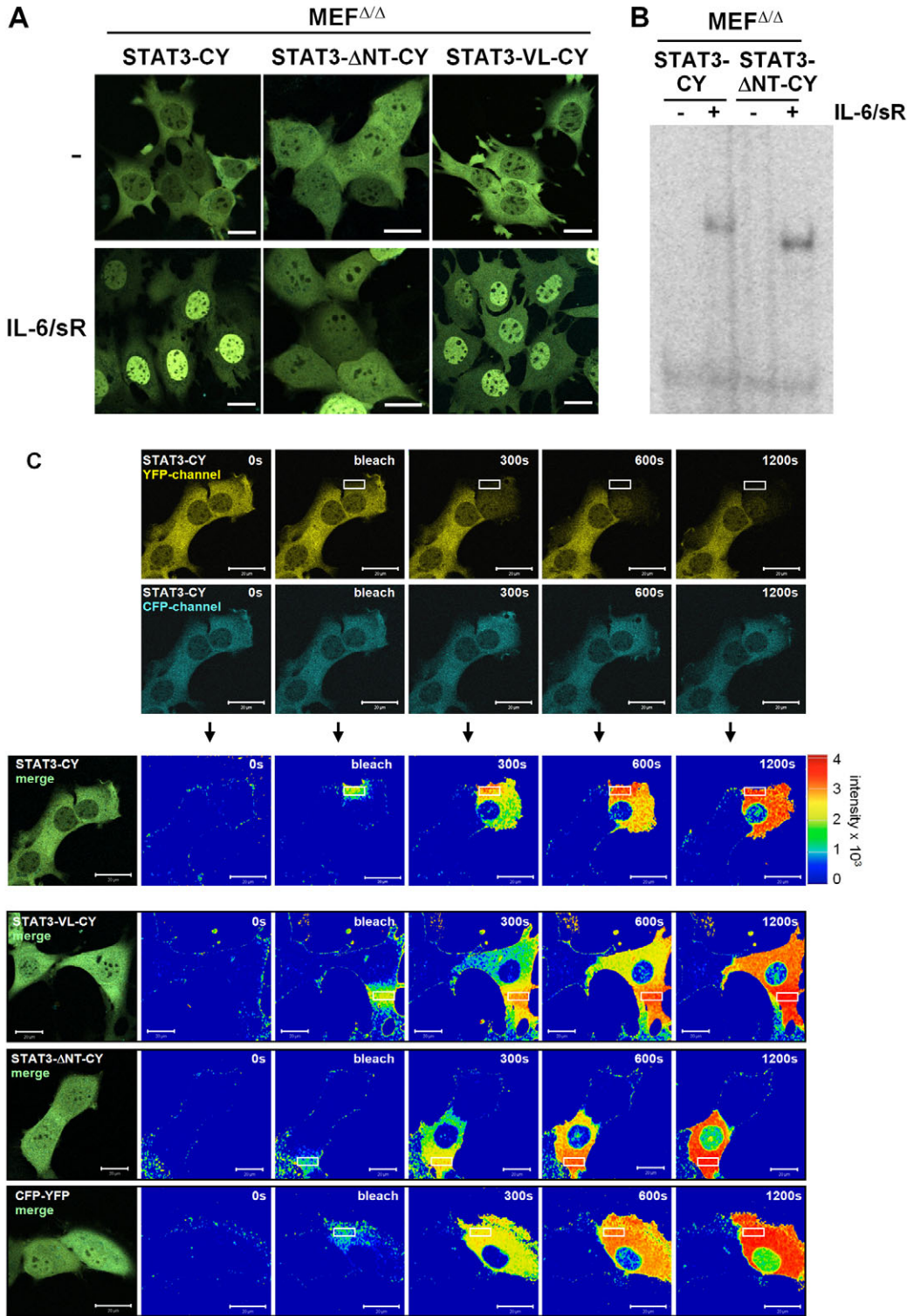


Fig. 6. Confocal analysis of N-terminal STAT3 mutants. (A) MEF $\Delta\Delta$ stably transfected with STAT3-CY, STAT3- Δ NT-CY or STAT3-VL-CY were stimulated with 20 ng/ml IL-6 and 0.5 μ g/ml soluble IL-6R (sR) for 30 minutes or left untreated. Living cells were analysed by confocal microscopy. (B) MEF $\Delta\Delta$ stably transfected with STAT3-CY or STAT3- Δ NT-CY were stimulated with 20 ng/ml IL-6 and 1 μ g/ml soluble IL-6R (sR) for 30 minutes or left untreated. Nuclear extracts were prepared and analysed in an electrophoretic mobility shift assay using hybridized 32 P-labelled oligonucleotides that form a STAT3 binding site. (C) Imaging of nucleocytoplasmic shuttling of STAT3-CY, STAT3-VL-CY, STAT3- Δ NT-CY and CFP-YFP in stably transfected MEF $\Delta\Delta$. Living cells were analysed in an incubation chamber at 37°C at a confocal microscope. The YFP and CFP channels of the confocal microscope were adjusted so that the YFP and CFP fluorescence of the STAT3-CY constructs appeared with the same intensities. For each pixel of the image, the intensities of the YFP and CFP fluorescence were used to calculate a new image that represented only YFP bleached molecules. Intensities are shown in rainbow colours, with blue representing weak and red strong signals. White rectangles represent the bleach ROIs used for the generation of YFP bleached STAT3-CY molecules. Scale bars: 20 μ m.

consequence of this algorithm, bleaching of YFP leads to the generation of a signal. The fate of the signal representing YFP-bleached molecules can be followed over time throughout the cell. Neighbouring non-bleached cells serve as controls. The YFP-bleached population of STAT3-CY rapidly diffused through the cytoplasm, the nuclear and the plasma membranes being barriers for free diffusion. However, over time a signal was detectable within the nucleus, indicating that a fraction of molecules passed

the nuclear membrane. STAT3-VL-CY behaved similarly to STAT3-CY (Fig. 6C, second merge panel). Compared to the two previous constructs, cytoplasmic bleaching of STAT3- Δ NT-CY resulted in a stronger nuclear signal after 20 minutes (Fig. 6C, third merge panel). Diffusion of the bleached CFP-YFP control was also hindered by the nuclear envelope. However, this construct showed the most pronounced nuclear presence after 20 minutes (Fig. 6C, lower panel).

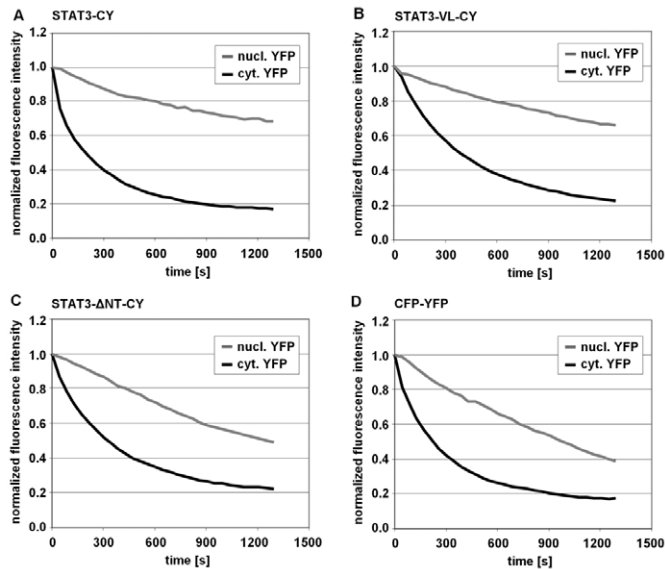


Fig. 7. Nucleocytoplasmic shuttling of STAT3 constructs in stably transfected MEF $\Delta\Delta$. (A–D) Living MEF $\Delta\Delta$ stably transfected with STAT3–CY (A), STAT3–VL–CY (B), STAT3– Δ NT–CY (C) and CFP–YFP (D) were analysed in an incubation chamber at 37°C at a confocal microscope as described for Fig. 6C. The diagrams show the normalized and averaged YFP fluorescence in cytoplasmic and nuclear ROIs over time from ten experiments for each construct. Only experiments with constant nuclear CFP fluorescence (not shown) were evaluated.

Ten measurements as depicted in Fig. 6C were performed for each of the four constructs. For quantitative evaluation of the data a cytoplasmic and a nuclear ROI were positioned. The diagrams in Fig. 7 show the averaged normalized cytoplasmic and nuclear fluorescence in these ROIs for each construct. The decay of nuclear YFP fluorescence upon cytoplasmic bleaching of YFP is indicative for nucleocytoplasmic shuttling. The decrease in nuclear YFP fluorescence of STAT3– Δ NT–CY (Fig. 7C) was steeper than in case of the other two STAT3 constructs, indicating that STAT3– Δ NT–CY shuttled more rapidly than STAT3–CY (Fig. 7A) and STAT3–VL–CY (Fig. 7B). As evident from the selected images in Fig. 6C, the CFP–YFP control (Fig. 7D) shuttled even faster than STAT3– Δ NT–CY.

Discussion

Although nucleocytoplasmic shuttling of latent STAT3 and nuclear accumulation of activated (i.e. tyrosine phosphorylated) STAT3 are well established, the molecular mechanisms driving these processes are ill-defined. The subcellular distribution of latent STAT3 with high cytoplasmic and low nuclear concentrations represents a steady state resulting from continuous nuclear import and export (Pranada et al., 2004). Treatment of cells with leptomycin B, an inhibitor of CRM1 (also known as exportin-1), leads to a partial nuclear accumulation of STAT3, indicating that latent nuclear export is in part dependent on CRM1 (Bhattacharya and Schindler, 2003).

To assess the role of CRM1-dependent nuclear export sequences for nucleocytoplasmic shuttling of latent STAT3, we mutated a putative NES sequence (QL₅₂₅TTL₅₂₈AEKLL) previously identified to be important for nuclear export of latent STAT3 (Bhattacharya and Schindler, 2003). As previously described, the resulting L525A/L528A mutant is enriched in the nuclei of resting cells and

accumulates in the nucleus upon stimulation. Unexpectedly, the L525A/L528A mutant shuttles faster between cytoplasm and the nucleus arguing against an impairment of CRM1-mediated export by this mutation. The increased shuttling rate suggests that the nuclear accumulation of this mutant is caused by enhanced nuclear import rather than perturbed export.

The recently solved structure of CRM1 in complex with ranGTP and the export substrate snurportin1 shows that the hydrophobic residues of an NES must be exposed for binding to a hydrophobic pocket of CRM1 (Monecke et al., 2009). Using the structure of the core fragment of STAT3 as a template (Ren et al., 2008), we found that the amino acids L525 and L528 are located on the back of an α -helix in the linker domain of STAT3 (supplementary material Fig. S1). Thus, these residues are buried and the mutations probably have an impact on the integrity of the domain instead of targeting a functional NES. The same is true for other putative NES sequences identified in the DNA-binding domain and the coiled-coil domain of STAT3 (supplementary material Figs S2 and S3). Therefore, the effect of leptomycin B on the subcellular distribution of STAT3 might not be mediated by acting on STAT3 directly, but possibly on another protein involved in CRM1-mediated export of STAT3. Another possibility is that the NES of STAT3 that interacts with CRM1 has not been identified yet.

Unfortunately, the role of NLS for the nuclear import of activated STAT3 is far from clear. A recent study on STAT1 suggests that a phosphorylated STAT1 dimer interacts in a nonconventional manner with importin α 5 without the involvement of a classical NLS (Nardozi et al., 2010). Several putative NLS within STAT3 have been defined by mutagenesis studies: R214/R215 and R414/417 by Ma and colleagues (Ma et al., 2003) and amino acids 150–163 by Liu and colleagues (Liu et al., 2005). However, in some of these studies an impact of the mutation on the integrity of the STAT3 protein cannot be excluded. One of these putative NLS comprising R214 and R215 of STAT3 has been shown to be essential for interaction of STAT3 with importin α 5 and for nuclear accumulation in response to tyrosine phosphorylation (Ma and Cao, 2006). In another report, the R214A/R215A mutant was described as showing increased CRM1-dependent nuclear export and a rim-like nuclear staining pattern (Sato et al., 2005). However, our data do not support these observations. R214 and R215 are part of a long α -helix within the coiled-coil domain of STAT3, one being exposed and the other buried (supplementary material Fig. S4). Mutation of these residues in the context of STAT3–CY did not change the subcellular distribution of STAT3 in resting cells but, as reported previously, impaired nuclear accumulation upon activation. The rate of nucleocytoplasmic shuttling was not affected by the mutation of R214 and R215. From this finding, we conclude that nucleocytoplasmic shuttling of latent STAT3 is independent of binding to importin. Possibly, nuclear import of latent STAT3 is facilitated by the direct interaction of STAT3 with constituents of the nuclear pore complex, as has been reported for STAT1 (Marg et al., 2004).

In the second part of our work, we elucidated the importance of dimerization of latent STAT3 for nucleocytoplasmic shuttling. The dimer interface of latent STAT3 has not been identified yet. From recent advances in the understanding of the dimerization of latent STAT1 (Mao et al., 2005) and the crystal structure of the STAT3 core fragment (Ren et al., 2008), we concluded that the N-terminal domain might be important for dimerization of latent STAT3. Indeed, deletion of the N-terminal domain of STAT3 abrogated dimer formation, as shown by bnPAGE and 2f-FCS. Point

mutations analogous to those that disturb homotypic interaction of the N-terminal domain of STAT1 had no detrimental effect on the dimerization of STAT3. It has recently been shown that the homotypic interaction of the N-terminal domains of STAT1 and STAT3 are of high and low affinity, respectively (Wenta et al., 2008). Therefore, the N-terminal domain of STAT3 might not contribute to STAT3 dimerization by homotypic interaction but by reciprocal interactions with another domain of STAT3. The SH2-domain could be a candidate for an interaction with the N-terminal domain because it has been shown that mutation of the SH2-domain affects dimer formation of unphosphorylated STAT3 (Kretzschmar et al., 2003). Such an interaction would lead to an antiparallel orientation of the latent STAT3 dimer, in contrast to the parallel orientation of the activated STAT3 dimer (Becker et al., 1998). The fact that monomeric latent STAT3- Δ NT shuttles between the nucleus and the cytoplasm indicates that dimerization of latent STAT3 is not required for nucleocytoplasmic shuttling. STAT3- Δ NT shuttles faster than the wild-type, suggesting that dimerization might even hinder nucleocytoplasmic shuttling of latent STAT3.

STAT3 lacking the N-terminal domain becomes phosphorylated and dimerizes in response to IL-6 stimulation. Thus, latent dimerization is not required for activation of STAT3 at the receptor. Furthermore, the N-terminal domain is not essential for the dimerization of phosphorylated STAT3. Activated STAT3 that lacks the N-terminal domain binds to DNA (Zhang and Darnell, 2001) (Fig. 6B). From the crystal structure of the phosphorylated STAT3 core fragment (lacking the N-terminal domain) bound to DNA it is evident that dimerization is mainly driven by phosphotyrosine-SH2 domain interactions and stabilized by DNA-binding (Becker et al., 1998). The result that phosphorylated STAT3 dimers lacking the N-terminal domain do not accumulate in the nucleus was unexpected (Zhang et al., 2006). However, a similar contribution of the N-terminal domain for nuclear accumulation has been shown for STAT1 (Meissner et al., 2004). These findings point to a functional role of the N-terminal domain for nuclear import of activated STAT3 that deserves further investigation.

Materials and Methods

Recombinant plasmids

The expression vector pSVL-STAT3-CY described previously (Pranada et al., 2004) served as a basis for cloning pcDNA5/FRT/TO-STAT3-CY using the pcDNA5/FRT/TO vector of the Flp-In system (Invitrogen). pcDNA5/FRT/TO-STAT3-CY was used as template for cloning the constructs STAT3- Δ NLS-CY, STAT3- Δ NES-CY, STAT3-VL-CY and STAT3- Δ NT-CY.

The STAT3 point mutants were generated by PCR with the following primers: R214A/R215A, sense 5'-CAGATGGCGGCAAGCATTG-3' and antisense 5'-CAATGCTTGCCGCCATCTG-3'; L525A/L528A, sense 5'-AGGCGACAACGGCGGCTGAGAAGC-3' and antisense 5'-CAGCCGCGTTGTCGCCTGCTCG-3'; V77A/L78A, sense 5'-GAGTCCAATGCCGCTATCAGCAC-3' and antisense 5'-GTGCTGATAGGCGGCATTGGACTC-3'. The deletion mutant Δ NT encoding amino acids 126-770 of STAT3 was generated by PCR introducing a *Xho*I site and a start codon with the sense primer 5'-TATTCTCGAGATGCAGCAAGGGGGC-CAGGCCAA-3'. The products were analysed and cloned into pcDNA5/FRT/TO-STAT3-CY. For cloning of CFP-YFP, STAT3-CY was used as a template and a *Xho*I site and a start codon was introduced by PCR with the sense primer 5'-ATCCGCTC-GAGCGCTACCGGTGCCAC-3'. The product was sequenced and transferred into pcDNA5/FRT/TO. The eGFP-labelled constructs were generated by replacing the CY-tag with eGFP. eGFP was expressed using the pEGFP-N1 vector (Invitrogen).

Cytokines and cytokine receptors

Recombinant human IL-6 was expressed in *Escherichia coli*, refolded, and purified as described previously (Arcone et al., 1991). The specific activity of IL-6 was measured by a B9 cell proliferation assay. sIL-6R α was expressed in insect cells as previously described (Weiergraber et al., 1995).

Cell culture and transfection

Murine embryonal fibroblasts MEF^{n/n} and MEF ^{$\Delta\Delta$} (generous gifts of Valeria Poli, University of Turin, Torino, Italy) were grown in Dulbecco's modified Eagle's medium

(DMEM) with GlutaMax (Invitrogen) supplemented with 10% FCS, 100 U/ml penicillin and 100 μ g/ml streptomycin (BIO-Whittaker, Verviers, Belgium). COS-7 cells were cultivated in phenol-red-free DMEM with 10% FCS. The cells were incubated at 37°C in a water-saturated atmosphere at 5% CO₂. MEF ^{$\Delta\Delta$} cells were stably reconstituted with STAT3-CY, STAT3- Δ NLS-CY, STAT3- Δ NES-CY, STAT-VL-CY, STAT3- Δ NT-CY or CFP-YFP using the Flp-In system (Invitrogen), ensuring integration of the different constructs at the same locus.

Preparation of cell lysates, SDS-PAGE and immunoblotting

MEF cells were cultured on six-well plates. The cells were stimulated with 20 ng/ml IL-6 and 500 ng/ml sIL-6R α for 30 minutes or left untreated. Subsequently, cells were lysed with RIPA lysis buffer (50 mM Tris-HCl pH 7.4, 150 mM NaCl, 1 mM EDTA, 0.5% Nonidet P-40, 1 mM NaF, 15% glycerol, 20 mM β -glycerophosphate, 1 mM Na₃VO₄, 0.25 mM phenylmethylsulfonyl fluoride (PMSF), 5 g/ml aprotinin and 1 g/ml leupeptin). The lysates were analysed by SDS-PAGE, western blotting and immunodetection using antibodies directed against phosphotyrosine 705 of STAT3 (Cell Signaling Technology, Danvers, MA), STAT3 (H190; Santa Cruz Biotechnology, Santa Cruz, CA), GAPDH (Santa Cruz Biotechnology) and horseradish-peroxidase-conjugated secondary antibodies (Dako, Hamburg, Germany). All antibodies were used in a 1:1000 dilution in TBS-N buffer (20 mM Tris-HCl, pH 7.6, 137 mM NaCl and 0.1% Nonidet P-40) and detected by chemiluminescence (ECL; Millipore, Billerica, MA).

Blue-native PAGE and detection of CFP and YFP

MEF cells were cultured on 10-cm dishes. The cells were stimulated with 25 ng/ml IL-6 and 500 ng/ml sIL-6R α for 30 minutes or left untreated. The cells were lysed in Brij-96V lysis buffer (0.1 M phosphate buffer pH 8.0, 0.5% Brij-96V, 1.5% glycerol, 0.5 mM EDTA, 1 mM Na₃VO₄, 0.25 mM PMSF, 5 g/ml aprotinin, and 1 g/ml leupeptin). The lysates were incubated with Coomassie Brilliant Blue G-250 (Serva, Heidelberg, Germany) to a final concentration of 0.2% and separated by blue-native PAGE (Schagger et al., 1994) using a gradient polyacrylamide gel (4-20%). The cathode buffer was composed of 50 mM Tricine, 15 mM BisTris and 0.02% Coomassie Brilliant Blue G-250; the anode buffer contained 50 mM BisTris-HCl pH 7. YFP fluorescence was analysed with a Typhoon gel fluorescence scanner (Amersham Biosciences) by excitation with a 488 nm laser line. The emission was detected using a 515-555 nm bandpass filter.

Preparation of nuclear extracts and electrophoretic mobility shift assay (EMSA)

After stimulation, the MEF were washed twice and harvested with PBS containing sodium vanadate. The pellet was resuspended in buffer A (10 mM HEPES-KOH pH 7.9, 1.5 mM MgCl₂, 10 mM KCl, 0.5 mM DTT, 0.2 mM PMSF, 1 mM sodium vanadate), sonified for 10 seconds, incubated 10 minutes on ice and centrifuged for 10 seconds at 16,000 g. The pellet was resuspended in buffer C (20 mM HEPES-KOH pH 7.9, 420 mM NaCl, 1.5 mM MgCl₂, 0.2 mM EDTA, 25% glycerol, 0.5 mM DTT, 0.2 mM PMSF, 1 mM sodium vanadate), incubated 20 minutes on ice and centrifuged for 2 minutes at 16,000 g. Protein concentrations of the supernatants were measured using the Bio-Rad protein assay (Bio-Rad, Richmond, CA). A double-stranded mutated *sis*-inducible element (SIE) oligonucleotide from the *c-fos* promoter (m67SIE: 5'-GATCCGGGAGGGATTACGGGAAATGCTG-3') was labelled by filling in 5'-protruding ends with the Klenow enzyme using [α -³²P]dATP. Nuclear extracts containing 3.5 μ g protein were incubated with about 10 fmol (10,000 cpm) of labelled oligonucleotides in gel shift incubation buffer (10 mM HEPES pH 7.8, 1 mM EDTA, 5 mM MgCl₂, 10% glycerol, 5 mM DTT, 2 mM PMSF, 0.05 mg/ml of poly(dI-dC) and 1 mg/ml BSA) for 10 minutes at room temperature. The DNA-protein complexes were separated on a 4.5% polyacrylamide gel containing 7.5% glycerol in 0.25% TBE buffer (200 mM Tris, 166 mM boric acid, 2 mM EDTA, adjusted to pH 8.3) at 20 V/cm. The gel was fixed in 10% methanol and 10% acetic acid for 15 minutes, dried and analysed by autoradiography.

Indirect immunofluorescence

MEF cells were grown on glass coverslips, washed twice with phosphate-buffered saline (PBS) containing 1 mM MgCl₂ and 0.1 mM CaCl₂ (PBS⁺⁺) and fixed with -20°C cold methanol for 15 minutes. Subsequently, the cells were permeabilized with PBS⁺⁺ containing 0.1% Triton X-100 (PBST⁺⁺) for 5 minutes, quenched with 50 mM NH₄Cl in PBST⁺⁺ and blocked with PBST⁺⁺ containing 1% BSA (Serva). Immunostaining was performed using a STAT3 antibody (124H6; Cell Signaling Technology) and a secondary antibody conjugated with Cy2 (Jackson Immunoresearch, West Grove, PA). The antibodies were diluted 1:200 in PBST⁺⁺ containing 0.2% BSA. The cells were incubated for 60 minutes with the specific STAT3 antibody, washed twice with PBST⁺⁺ and incubated with the secondary antibody for 60 minutes. The coverslips were dipped in water and mounted with ImmuMount (Shandon, Sewickley, PA).

Confocal fluorescence microscopy and live cell imaging

Confocal imaging was performed with a Zeiss LSM 510Meta confocal microscope (Zeiss, Jena, Germany). CFP and YFP fluorescence were detected as described previously (Pranada et al., 2004). Cy2 fluorescence was detected using the 488 nm line of the argon laser, a 488 nm dichroic mirror and a 505-530 nm bandpass filter. The

images shown represent confocal slices of approximately 1 μm . The cells were examined with a 63×1.2 NA Zeiss water immersion objective. For fixation, stably transfected MEF^{ΔΔ} cells were grown on glass coverslips for 48 hours. The cells were fixed with 3.7% paraformaldehyde for 15 minutes and washed twice with PBS⁺⁺. Subsequently, the cells were quenched with 50 mM NH₄Cl in PBS⁺⁺ for 5 minutes, dipped in water and mounted with ImmuMount.

For live-cell imaging, stably transfected MEF^{ΔΔ} cells were grown on 42-mm glass coverslips. After 48 hours, the coverslips were placed into a thermostatted (37°C) and CO₂-controlled incubation chamber (Pecon, Erbach, Germany) and flushed with phenol-red-free DMEM (Invitrogen). iFLAP experiments were performed as described previously (Pranada et al., 2004). To analyse the shuttling by calculating the ratio of CFP and YFP fluorescence, the iFLAP method was modified (Herrmann et al., 2007). The CFP and YFP signals from STAT3-CY were adjusted to equal intensities. A signal was generated by bleaching the YFP moiety in a cytoplasmic ROI with the 514 nm line of the argon laser during data recording. Depicted intensities for YFP (iYFP) and CFP (iCFP) were calculated using the algorithm $(1 - iYFP/iCFP) \times 4096 = iYFP_{\text{bleach}}$ (12 bit picture) to give values representing only bleached YFP molecules.

Dual-focus fluorescence correlations spectroscopy (2f-FCS)

CO5-7 cells were transfected with 2 μg of plasmids encoding eGFP, STAT3-eGFP and STAT3-ΔNT-eGFP using Mirus TransIT-LT1 transfection reagent (Mirus Bio, Madison, WI). The cells were lysed in Brij-96V lysis buffer (as described above but lacking glycerol).

The 2f-FCS experiments were carried out using a setup based on a standard confocal epi-fluorescence microscope (Böhmer et al., 2001). eGFP and eGFP-tagged fusion constructs were excited with a 470 nm laser beam (LDH-P-C-470B). The fluorescent emission light was split from the excitation light by using a clearup bandpass filter (490–520 nm). The light was focused by confocal optics with a pinhole diameter of 200 μm onto a single photon avalanche diode (SPAD, PDM series, Micro Photon Devices, Bolzano, Italy). The temperature was controlled, using a home-made thermostatted device at 25°C (Müller and Rietinger, 2008).

An adequate model (Dertinger et al., 2007) for ACF/CCF is given by Eqn 1:

$$g(t, \delta, v) = \frac{c}{4} \sqrt{\frac{\pi}{Dt}} \int dz_1 \int dz_2 \frac{\kappa(z_1)\kappa(z_2)}{8Dt + w^2(z_1) + w^2(z_2)} \times \exp\left[-\frac{(z_2 - z_1 - v_z t)^2}{4Dt} - 2\frac{(\delta - v_x t)^2 + v_y^2 t^2}{8Dt + w^2(z_1) + w^2(z_2)}\right], \quad (1)$$

where δ is the lateral distance between the detection volume centres, t is the lag-time of correlation, v is particle velocity, x, y and z are Cartesian coordinates with z along the optical axis, c is the concentration of the fluorescent molecules and D is the diffusion coefficient. The functions of $\kappa(z)$ and $w(z)$ are given by Eqns 2–4:

$$w(z) = w_0 \left[1 + \left(\frac{\lambda_{\text{ex}} z}{\pi w_0^2 n} \right)^2 \right]^{1/2}, \quad (2)$$

and:

$$\kappa(z) = 2 \int_0^\alpha \frac{d\rho\rho}{R^2(z)} \exp\left(-\frac{2\rho^2}{R^2(z)}\right) = 1 - \exp\left(-\frac{2\alpha^2}{R^2(z)}\right), \quad (3)$$

with:

$$R(z) = R_0 \left[1 + \left(\frac{\lambda_{\text{em}} z}{\pi R_0^2 n} \right)^2 \right]^{1/2}, \quad (4)$$

where λ_{ex} and λ_{em} are excitation and emission wavelengths, n is the refractive index of the sample, α is the confocal pinhole radius, and w_0 and R_0 are fit parameters (Müller et al., 2008). 2f-FCS experiments were performed with three independent samples per construct and over 120 minutes detection time for each measurement point. The fitting procedure of experimental data was carried out globally for both the ACFs and CCF using a single particle diffusion model including triplet state correction (without the necessity to imply a dual particle diffusion model suggesting a second slow-moving component). Molecular mass estimation of the measured particles (assuming spherical symmetry) was calculated with the known molecular mass of eGFP (27 kDa) using Eqn 5:

$$MM_{\text{sample}} = \left(\frac{D_{\text{eGFP}}}{D_{\text{sample}}} \right)^3 \times MM_{\text{eGFP}}, \quad (5)$$

where MM is the molecular mass, and D is the diffusion coefficient from 2f-FCS experiments.

The project was supported by the Deutsche Forschungsgemeinschaft (SFB 542 projects B12 and Z1), the European Community (Marie Curie Research and Training Network ReceptEUR) and the excellence initiative of the German federal and state governments.

Supplementary material available online at <http://jcs.biologists.org/cgi/content/full/124/6/900/DC1>

References

- Arcone, R., Pucci, P., Zappacosta, F., Fontaine, V., Malorni, A., Marino, G. and Ciliberto, G. (1991). Single-step purification and structural characterization of human interleukin-6 produced in *Escherichia coli* from a T7 RNA polymerase expression vector. *Eur. J. Biochem.* **198**, 541–547.
- Becker, S., Groner, B. and Müller, C. W. (1998). Three-dimensional structure of the Stat3b homodimer bound to DNA. *Nature* **394**, 145–151.
- Bhattacharya, S. and Schindler, C. (2003). Regulation of Stat3 nuclear export. *J. Clin. Invest.* **111**, 553–559.
- Böhmer, M., Pampaloni, F., Wahl, M., Rahn, H. J., Erdmann, R. and Enderlein, J. (2001). Advanced time-resolved confocal scanning device for ultrasensitive fluorescence detection. *Rev. Sci. Instrum.* **72**, 4145–4152.
- Braunstein, J., Brutsaert, S., Olson, R. and Schindler, C. (2003). STATs dimerize in the absence of phosphorylation. *J. Biol. Chem.* **278**, 34133–34140.
- Dertinger, T., Pacheco, V., von der Hocht, I., Hartmann, R., Gregor, I. and Enderlein, J. (2007). Two-focus fluorescence correlation spectroscopy: a new tool for accurate and absolute diffusion measurements. *Chemphyschem* **8**, 433–443.
- Frahm, T., Hauser, H. and Köster, M. (2006). IFN-type-I-mediated signaling is regulated by modulation of STAT2 nuclear export. *J. Cell Sci.* **119**, 1092–1104.
- Haan, S., Kortylewski, M., Behrmann, I., Müller-Esterl, W., Heinrich, P. C. and Schaper, F. (2000). Cytoplasmic STAT proteins associate prior to activation. *Biochem. J.* **345**, 417–421.
- Herrmann, A., Vogt, M., Mönningmann, M., Clahsen, T., Sommer, U., Haan, S., Poli, V., Heinrich, P. C. and Müller-Newen, G. (2007). Nucleocytoplasmic shuttling of persistently activated STAT3. *J. Cell Sci.* **120**, 3249–3261.
- Kim, S. A. and Schwille, P. (2003). Intracellular applications of fluorescence correlation spectroscopy: prospects for neuroscience. *Curr. Opin. Neurobiol.* **13**, 583–590.
- Kretschmar, A. K., Dinger, M. C., Henze, C., Brocke-Heidrich, K. and Horn, F. (2003). Analysis of Stat3 dimerization by fluorescence resonance energy transfer in living cells. *Biochem. J.* **377**, 289–297.
- Levy, D. E. and Darnell, J. E., Jr (2002). Stats: transcriptional control and biological impact. *Nat. Rev. Mol. Cell Biol.* **3**, 651–662.
- Levy, D. E. and Lee, C. K. (2002). What does Stat3 do? *J. Clin. Invest.* **109**, 1143–1148.
- Liu, L., McBride, K. M. and Reich, N. C. (2005). STAT3 nuclear import is independent of tyrosine phosphorylation and mediated by importin- α 3. *Proc. Natl. Acad. Sci. USA* **102**, 8150–8155.
- Ma, J. and Cao, X. (2006). Regulation of Stat3 nuclear import by importin α 5 and importin α 7 via two different functional sequence elements. *Cell. Signal.* **18**, 1117–1126.
- Ma, J., Zhang, T., Novotny-Diermayr, V., Tan, A. L. and Cao, X. (2003). A novel sequence in the coiled-coil domain of Stat3 essential for its nuclear translocation. *J. Biol. Chem.* **278**, 29252–29260.
- Mao, X., Ren, Z., Parker, G. N., Sondermann, H., Pastorello, M. A., Wang, W., McMurray, J. S., Demeler, B., Darnell, J. E., Jr and Chen, X. (2005). Structural bases of unphosphorylated STAT1 association and receptor binding. *Mol. Cell* **17**, 761–771.
- Marg, A., Shan, Y., Meyer, T., Meissner, T., Brandenburg, M. and Vinkemeier, U. (2004). Nucleocytoplasmic shuttling by nucleoporins Nup153 and Nup214 and CRM1-dependent nuclear export control the subcellular distribution of latent Stat1. *J. Cell Biol.* **165**, 823–833.
- Meissner, T., Krause, E., Lodige, I. and Vinkemeier, U. (2004). Arginine methylation of STAT1: a reassessment. *Cell* **119**, 587–589.
- Meyer, T. and Vinkemeier, U. (2004). Nucleocytoplasmic shuttling of STAT transcription factors. *Eur. J. Biochem.* **271**, 4606–4612.
- Monecke, T., Guttler, T., Neumann, P., Dickmanns, A., Görlich, D. and Finer, R. (2009). Crystal structure of the nuclear export receptor CRM1 in complex with Snurportin1 and RanGTP. *Science* **324**, 1087–1091.
- Müller, C. B. and Rietinger, W. (2008). Sealed and temperature-controlled sample cell for inverted and confocal microscopes and correlation spectroscopy. *Colloid Polym. Sci.* **286**, 1215–1222.
- Müller, C. B., Loman, A., Pacheco, V., Koberling, F., Willibold, D., Rietinger, W. and Enderlein, J. (2008). Precise measurement of diffusion by multi-color dual-focus fluorescence correlation spectroscopy. *Eur. Phys. Lett.* **83**, 1–5.
- Nardozi, J., Wentha, N., Yasuhara, N., Vinkemeier, U. and Cingolani, G. (2010). Molecular basis for the recognition of phosphorylated STAT1 by importin α 5. *J. Mol. Biol.* **402**, 83–100.
- Pranada, A. L., Metz, S., Herrmann, A., Heinrich, P. C. and Müller-Newen, G. (2004). Real time analysis of STAT3 nucleocytoplasmic shuttling. *J. Biol. Chem.* **279**, 15114–15123.
- Ren, Z., Mao, X., Mertens, C., Krishnaraj, R., Qin, J., Mandal, P. K., Romanowski, M. J., McMurray, J. S. and Chen, X. (2008). Crystal structure of unphosphorylated STAT3 core fragment. *Biochem. Biophys. Res. Commun.* **374**, 1–5.
- Sato, N., Tsuruma, R., Imoto, S., Sekine, Y., Muromoto, R., Sugiyama, K. and Matsuda, T. (2005). Nuclear retention of STAT3 through the coiled-coil domain regulates its activity. *Biochem. Biophys. Res. Commun.* **336**, 617–624.
- Schägger, H., Cramer, W. A. and von Jagow, G. (1994). Analysis of molecular masses and oligomeric states of protein complexes by blue native electrophoresis and isolation of membrane protein complexes by two-dimensional native electrophoresis. *Anal. Biochem.* **217**, 220–230.

- Weiergräber, O., Hemmann, U., Küster, A., Müller-Newen, G., Schneider, J., Rose-John, S., Kurschat, P., Brakenhoff, J. P., Hart, M. H., Stabel, S. et al.** (1995). Soluble human interleukin-6 receptor: expression in insect cells, purification and characterization. *Eur. J. Biochem.* **234**, 661-669.
- Wenta, N., Strauss, H., Meyer, S. and Vinkemeier, U.** (2008). Tyrosine phosphorylation regulates the partitioning of STAT1 between different dimer conformations. *Proc. Natl. Acad. Sci. USA* **105**, 9238-9243.
- Yu, H. and Jove, R.** (2004). The STATs of cancer-new molecular targets come of age. *Nat. Rev. Cancer* **4**, 97-105.
- Zhang, L., Badgwell, D. B., Bevers, J. J., 3rd, Schlessinger, K., Murray, P. J., Levy, D. E. and Watowich, S. S.** (2006). IL-6 signaling via the STAT3/SOCS3 pathway: functional analysis of the conserved STAT3 N-domain. *Mol. Cell. Biochem.* **288**, 179-189.
- Zhang, X. and Darnell, J. E., Jr** (2001). Functional importance of Stat3 tetramerization in activation of the alpha 2-macroglobulin gene. *J. Biol. Chem.* **276**, 33576-33581.